A&A 472, 111–119 (2007)
DOI: 10.1051/0004-6361:20077631

Astronomy & Astrophysics

A search for ultra-compact dwarf galaxies in the Centaurus galaxy cluster⋆,⋆⋆

S. Mieske[1], M. Hilker[1], A. Jordán[1], L. Infante[2], and M. Kissler-Patig[1]

[1] European Southern Observatory, Karl-Schwarzschild-Strasse 2, 85748 Garching bei München, Germany
e-mail: [smieske; mhilker; ajordan; mkissler]@eso.org
[2] Departamento de Astronomía y Astrofísica, Pontificia Universidad Católica de Chile, Casilla 306, Santiago 22, Chile
e-mail: linfante@astro.puc.cl

Received 11 April 2007 / Accepted 14 June 2007

ABSTRACT

Aims. Our aim is to extend the investigations of ultra-compact dwarf galaxies (UCD) beyond the well studied Fornax and Virgo clusters.
Methods. We measured spectroscopic redshifts of about 400 compact object candidates with $19.2 < V < 22.4$ mag in the central region of the Centaurus galaxy cluster ($d = 43$ Mpc), using 3 pointings with VIMOS@VLT. The luminosity range of the candidates covers the bright end of the globular cluster (GC) luminosity function and the luminosity regime of UCDs in Fornax and Virgo. Within the area surveyed, our completeness in terms of slit allocation is ≈30%.
Results. We find 27 compact objects with radial velocities consistent with them being members of Centaurus, covering an absolute magnitude range $-12.2 < M_V < -10.9$ mag. We do not find counterparts to the two very large and bright UCDs in Fornax and Virgo with $M_V = -13.5$ mag, possibly due to survey incompleteness. The compact objects' distribution in magnitude and space is consistent with that of the GC population. Their kinematics and spatial distribution indicate that they are associated more to the central galaxies than to the overall cluster potential. The compact objects have a mean metallicity consistent with that of the metal-rich globular cluster sub-population. Compact objects with high S/N spectra exhibit solar [α/Fe] abundances, consistent with typical dwarf elliptical galaxy values and unlike galactic bulge globular clusters. HST based size estimates for a sub-sample of eight compact objects reveal the existence of one very large object with half-light radius r_h around 30 pc, having $M_V = -11.6$ mag ($\simeq 10^7\ M_\odot$). This source shows super-solar [α/Fe] abundances. Seven further sources are only marginally larger than typical GCs with r_h in the range 4 to 10 pc. Those sources exhibit a large scatter in [α/Fe] abundances.
Conclusions. We consider the largest compact object found to be the only bona fide UCD detected in our study. In order to improve our understanding of UCDs in Centaurus, a significant increase of our survey completeness is necessary.

Key words. galaxies: clusters: individual: Centaurus – galaxies: dwarf – galaxies: fundamental parameters – galaxies: nuclei – galaxies: star clusters

1. Introduction

In their spectroscopic studies of the Fornax galaxy cluster, Hilker et al. (1999) and Drinkwater et al. (2000 and 2003) reported on the discovery of six isolated compact stellar systems, having $-13.5 < M_V < -12$ mag and half-light radii r_h between 20 and 100 pc. Due to their compactness compared to dwarf galaxies of similar luminosity, they were dubbed "ultra-compact dwarf galaxies" (UCDs) (Phillipps et al. 2001). More recently, UCDs have also been discovered in the Virgo cluster (Haşegan et al. 2005; Jones et al. 2006).

There are, currently, two main hypotheses on the origin of UCDs: 1. UCDs are remnant nuclei of dwarf elliptical galaxies stripped in the potential well of their host cluster (e.g. Bassino et al. 1994; Bekki et al. 2003). 2. UCDs are merged stellar superclusters created in gas-rich galaxy mergers (e.g. Fellhauer & Kroupa 2002).

High resolution imaging and spectroscopy (Drinkwater et al. 2003; Hilker et al. 2007) place the Fornax UCDs between the sequence of globular clusters (GCs) and dwarf elliptical galaxies (dEs) in the fundamental plane of stellar systems. Their M/L ratios are in the range 2–5 and can be explained without invoking the presence of dark matter. The luminosities, sizes and M/L ratios of Fornax UCDs are comparable to those of bright nuclei of nucleated dwarf ellipticals (dE, Ns) (Lotz et al. 2004; Côté et al. 2006; Hilker et al. 2007).

For the Virgo cluster, Haşegan et al. (2005) report on three compact objects with M/L ratios between 6 and 9, suggesting such high ratios as a criterion to separate UCDs from GCs. From their HST based size estimates they furthermore derived a limit between normal GCs and larger sources (Dwarf Globular Transition Objects in their notation) to occur at about $2\times10^6\ M_\odot$. Evstigneeva et al. (2007) find that Virgo UCDs are in general more α enriched than dwarf elliptical galaxies in Fornax and Virgo. This is not naturally explained by the hypothesis that Virgo UCDs are dominated by stripped nuclei.

Our long term aim is to characterise UCD properties in a broad range of environments (e.g. Mieske et al. 2004b; Mieske et al. 2006c). For the Fornax cluster (Mieske et al. 2002, 2004a) we have shown that the luminosity distribution of compact objects for $M_V < -10.4$ mag does not show any discontinuities that would hint at two separate populations (i.e. UCDs vs.

⋆ Based on observations obtained in service mode at the VLT (programme 076.B-0293).
⋆⋆ Table 1 is only available in electronic form at http://www.aanda.org

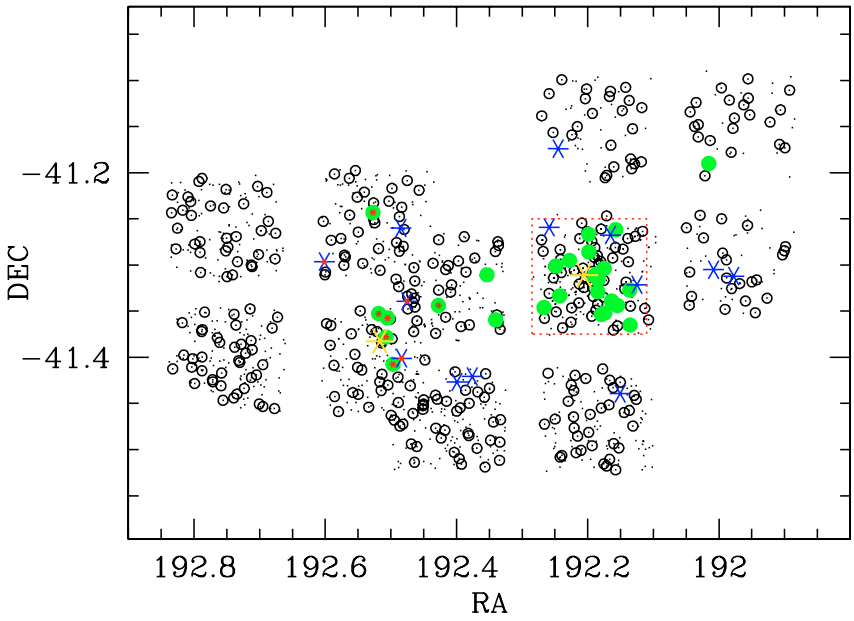

Fig. 1. Map of the VIMOS observations in the Centaurus cluster. Dots are all photometrically selected compact object candidates from the VIMOS pre-images. Open circles mark the 386 compact objects with measured radial velocities (out of 405 for which slits had been allocated). Filled (green) circles indicate the 27 compact objects with radial velocities in the range of the Centaurus cluster ($1750 < v_{\rm rad} < 5550$ km s^{-1}, see Fig. 3). Filled (green) circles with red dots indicate objects with radial velocity above 4000 km s^{-1}, hence members of the Cen45 sub-cluster. Blue asterisks indicate the locations of 13 dwarf elliptical galaxies included in this study. The golden asterisks indicate the location of NGC 4696 and NGC 4709, the central galaxies of the Cen30 and Cen45 components. The dotted red rectangle indicates the central FORS pointing of our deep photometric Centaurus cluster study (see text and Mieske et al. 2005).

GCs)[1]. Only the brightest UCD with $M_V = -13.5$ mag clearly stands out. In Mieske et al. (2006a), we found a break in the metallicity distribution at $M_V = -11$ mag, such that brighter compact objects are more metal rich than fainter compact objects. Furthermore, we identified a change in the size-luminosity relation occurring at about the same luminosity, similar to the Virgo cluster case. Fainter sources have luminosity independent half light radii of $r_{\rm h} \simeq 3$pc (e.g. Jordán et al. 2005), brighter sources have sizes correlating with their luminosity (Haşegan et al. 2005; Kissler-Patig et al. 2006). We therefore identified $M_V = -11$ mag ($\sim 3\times10^6\ M_\odot$) as the rough dividing line between GCs and UCDs in Fornax. Nuclear regions of Fornax dE,Ns were found to be about 0.6 dex more metal poor than Fornax UCDs, implying that Fornax UCDs do probably not originate from the current population of dE,Ns.

The Centaurus cluster of galaxies ($(m - M) = 33.28$ mag or 43 Mpc, Mieske et al. 2005) is the most nearby southern cluster of mass comparable to Virgo ($m \simeq 5 \times 10^{14}\ M_\odot$, Reiprich & Böhringer 2002). It is therefore a natural target for broadening the environmental baseline of UCD investigations. The Centaurus cluster consists of a main component Cen30 at $v_{\rm rad} \simeq 3000$ km s^{-1}, dominated by NGC 4696, and an in-falling, spiral-rich subcomponent at $v_{\rm rad} \simeq 4500$ km s^{-1}, called Cen45 (Stein et al. 1997), which is dominated by NGC 4709.

In this paper, we present a spectroscopic search for UCDs in the Centaurus cluster, which we term Centaurus Compact Object Survey "CCOS".

2. The data

The data for this publication were obtained in service mode with the VIsible MultiObject Spectrograph VIMOS (Le Fevre et al. 2003) mounted on UT3 Melipal at the VLT (programme 076.B-0293). VIMOS allows simultaneous observing of 4 quadrants, each of dimension $7' \times 8'$, and separated by about $2'$. We observed three multi-object spectroscopy (MOS) pointings in the central Centaurus cluster, covering both NGC 4696 and NGC 4709 (see Fig. 1).

[1] we refer as "compact objects" to sources in the magnitude regime of bright globular clusters and Fornax UCDs. Only if the properties of a compact object cannot be explained by the general globular cluster population, we refer to it as UCD. In our usage the term UCD does not imply a particular formation channel.

2.1. Candidate selection

The candidates for our survey were selected from the VIMOS pre-imaging that was performed in the V and R filters.

For de-redenning the apparent magnitudes we used Schlegel et al. (1998). To select sources as compact object candidates, we defined three criteria regarding size, colour and luminosity.

1. Be unresolved on the VIMOS pre-imaging (as judged by SExtractor star-classifier, Bertin & Arnouts 1996). The PSF $FWHM$ typically was 0.8″, corresponding to ≈150 pc at the distance of Centaurus.
2. Have de-redenned colours $0.23 < (V - R)_0 < 0.73$ mag, in order to cover a broad metallicity range for old stellar populations ($-3 \leq$ [Fe/H] ≤ 0.5 dex for a 13 Gyr population, Bruzual & Charlot 2003).
3. Have de-redenned apparent magnitudes $19.2 < V_0 < 22.4$ mag ($-14.1 < M_V < -10.9$ mag). This covers both the bright end of the globular cluster luminosity function (GCLF) and the magnitude range of all UCDs discovered so far.

2.2. Spectroscopic observations

Within our 12 masks (3 pointings × 4 quadrants) the VIMOS mask creation software VMMPS enabled the allocation of 405 compact objects (minimum slit length 6″), compared to a total of 1340 photometrically selected sources. We were able to measure redshifts for 386 out of those 405 sources. Our completeness in the area surveyed is hence about 29%. We furthermore added 13 early-type dwarf galaxies in the range $-16.2 < M_B < -13.9$ mag to the masks, all from the Centaurus Cluster Catalog (Jerjen et al. 1997). Nine of those were already known members from radial velocity measurements (Stein et al. 1997).

We used the medium resolution MR grism with the order sorting filter GG475. This covers the wavelength range from 4800 to 10 000 Å at a dispersion of 2.5 Å per pixel. The average seeing for the spectroscopic observations was around 0.8″,

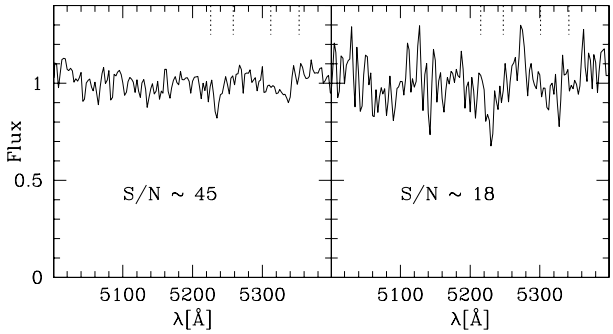

Fig. 2. Example excerpts of two reduced spectra of Centaurus compact objects. The dashed ticks at the top mark the correspondingly red-shifted regions of the Mgb and Fe5270 Lick indices. *Left*: object CCOS J1248.54-4119.64, with a S/N around 45. *Right*: object CCOS J1248.74-4118.95, with a S/N around 18.

at a slit width of 1.0″. With a pixel scale of 0.2″, the instrumental resolution ($FWHM$) is 10–12 Å, at about the limit for Lick index measurements. For each pointing the total exposure time was 8400 s, subdivided in four single exposures of 2100 s.

Arc-lamp exposures for wavelength calibration were taken for every second science exposure. We also observed four Lick standard stars (HD 064606, HD 131976, HD 131977, HD 148816) with the same grism and slit width as the science exposures.

3. Data reduction

For the data reduction from 2D raw spectrum to wavelength calibrated 1D spectrum we used the recipes vmmosobsjitter and vmmosobsstare provided by the ESO VIMOS pipeline[2]. These recipes perform bias subtraction, flat field division, wavelength calibration, image combination (only for vmmosobsjitter), and spectrum extraction.

The radial velocity measurements of the calibrated 1D spectra were performed via cross-correlation using the IRAF task fxcor in the *RV* package. As template for cross-correlation we used a synthetic spectrum created to resemble a typical early-type galaxy (see also Mieske et al. 2002).

For the cluster membership determination we measured the radial velocity on the 1D spectrum combined from the four single exposures with the recipe vmmosobsjitter. The S/N per pixel in these spectra was in the range 12 to 63 in the wavelength range of highest transmission (6700 to 6800 Å). The radial velocity measurement errors were of the order 50–100 km s^{-1}. As a cluster membership criterion we required $1750 < v_{\rm rad} < 5550$ km s^{-1}, excluding both foreground stars and background galaxies (see Fig. 3). This resulted in the discovery of 40 cluster members, comprised by 27 compact cluster members and the 13 dEs (see Tables 1 and 2). Example spectra for two Centaurus compact objects are shown in Fig. 2.

In order to refine the velocity measurements, we compared the radial velocities derived from the combined exposures with those derived from the single science exposures that were observed back-to-back with an arc-lamp exposure. This comparison showed no systematic difference in quadrants 3 and 4 to a level of 30 km s^{-1}. For quadrants 1 and 2 the velocity derived from the two exposures next to the wave-lamp was higher by about 100 km s^{-1} for quadrant 1 and lower by about 100 km s^{-1} for quadrant 2. We attribute these offsets to the well-known flexure of the VIMOS instrument. In order to determine the final radial velocity, we corrected the mean velocity in quadrants 1 and 2 by those shifts, and adopted the uncorrected mean for quadrants 3 and 4.

[2] http://www.eso.org/projects/dfs/dfs-shared/web/vimos/vimos-pipe-recipes.html

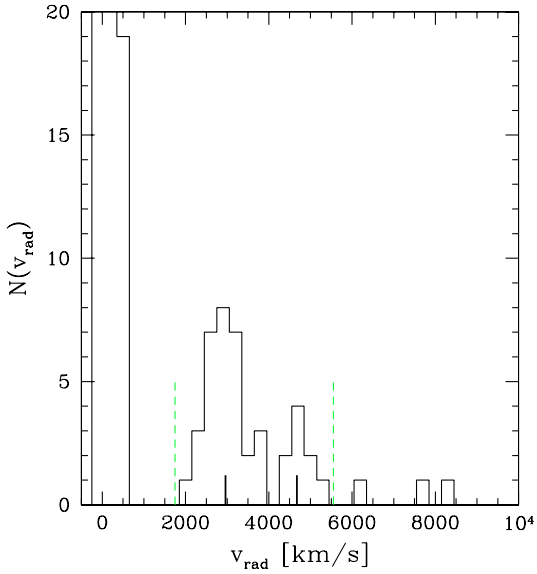

Fig. 3. Radial velocity histogram of all observed sources. The green dashed lines mark the limits applied for Centaurus cluster membership selection (40 Centaurus cluster members, including 13 dEs). The two vertical ticks mark the radial velocities of NGC 4696 (~3000 km s^{-1}) and NGC 4709 (~4500 km s^{-1}).

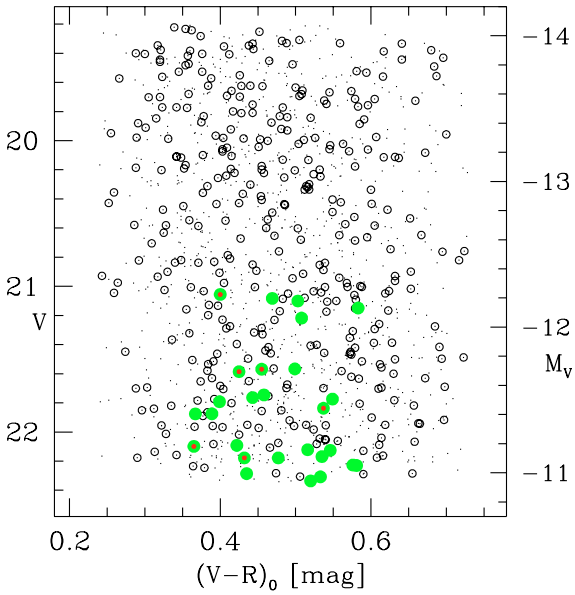

Fig. 4. Colour-magnitude diagram in VR of the sources from Fig. 1, excluding the dwarf elliptical galaxies.

4. Results

Out of the 386 compact objects with measurable redshift observed, 27 turn out to be Centaurus cluster members (see Fig. 3 and Table 1). In the following subsections we will investigate their photometric properties, spatial distribution, abundances, kinematics, and their structural parameters. The null hypothesis is that their properties can be explained by the Centaurus cluster globular cluster systems.

Table 2. Properties of the 13 Centaurus cluster dEs observed in our study. The first column gives the identifier from the Centaurus cluster catalog (CCC, Jerjen et al. 1997). The B_T magnitude is from the CCC, all other observables are from this study. The last column gives the radial velocity measured for 9 of the 13 sources by Stein et al. (1997).

ID	RA (J2000)	Dec (J2000)	B_T	v_{rad} [km s^{-1}]	⟨Fe⟩ [Å]	Mgb [Å]	$v_{rad,S97}$ [km s^{-1}]
CCC 125	12:49:56.31	−41:15:35.97	17.14	3016 (78)	2.85 (0.34)	4.18 (0.45)	2880 (35)
CCC 61	12:48:39.68	−41:16:03.14	17.40	2871 (62)	3.72 (0.12)	4.14 (0.17)	2910 (67)
CCC 58	12:48:36.20	−41:26:21.38	17.94	3312 (58)	3.20 (0.23)	3.65 (0.33)	3304 (60)
CCC 22	12:48:02.05	−41:18:18.25	17.94	2467 (38)	2.79 (0.09)	3.90 (0.13)	2433 (33)
CCC 75	12:49:02.05	−41:15:33.26	18.06	1977 (73)	3.34 (0.19)	3.62 (0.26)	1958 (71)
CCC 150	12:50:24.36	−41:17:46.91	18.23	4408 (99)	2.49 (0.15)	3.07 (0.20)	4426 (46)
CCC 104	12:49:35.82	−41:25:36.59	18.25	3317 (75)	3.54 (0.47)	4.89 (0.65)	–
CCC 121	12:49:54.15	−41:20:21.39	18.36	4661 (62)	1.55 (0.30)	2.96 (0.41)	4739 (70)
CCC 52	12:48:29.99	−41:19:16.93	18.42	3768 (73)	3.59 (0.27)	4.05 (0.37)	–
CCC 123	12:49:56.03	−41:24:04.06	18.45	4729 (46)	2.42 (0.14)	2.75 (0.20)	4661 (69)
CCC 97	12:49:30.19	−41:25:14.93	18.70	2870 (70)	3.58 (0.19)	4.63 (0.25)	2818 (30)
CCC 72	12:48:58.81	−41:10:26.55	19.11	3218 (54)	2.74 (0.27)	2.20 (0.37)	–
CCC 16	12:47:54.58	−41:18:43.37	19.40	3891 (58)	2.78 (0.19)	3.27 (0.27)	–

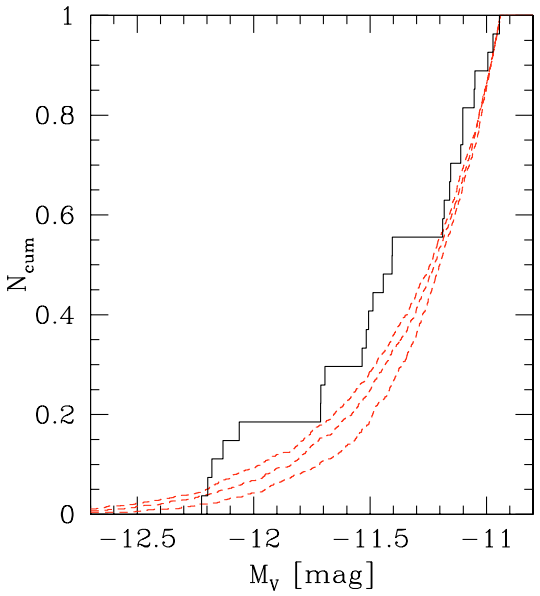

Fig. 5. Cumulative magnitude distribution of Centaurus compact objects. Dashed lines indicate the cumulative magnitude distribution of assumed Gaussian Globular Cluster Luminosity Functions with three different widths σ: from top to bottom 1.4, 1.3, and 1.2 mag. The assumed turnover magnitude is $M_V = -7.4$ mag. The KS-test probabilities with which the measured compact object distribution is drawn from the Gaussians are 21% (σ = 1.4 mag), 11% (σ = 1.3 mag) and 2% (σ = 1.2 mag).

4.1. Photometry

Figure 4 shows a colour-magnitude diagram in *VR* of all compact cluster members, all observed objects, and all photometrically selected objects. It suggests that no detection bias was introduced by our colour selection.

A first step to test our null hypothesis is to compare the cumulative magnitude distribution of the compact objects with that expected for a generic globular cluster luminosity function (GCLF). For very bright galaxies like NGC 4696 and NGC 4709, the typical dispersion (σ) of a Gaussian GCLF is around 1.3 to 1.4 mag (Jordan et al. 2006, 2007; Kundu & Whitmore 2001). Figure 5 shows that for such values, the agreement with our data is still at the 10–20% level according to a KS-test. Only with respect to an assumed width of σ = 1.2 mag, the agreement drops to 2%.

A further test is to estimate the total number of UCDs one would expect to detect in the case of the stripping scenario. Bekki et al. (2003) predict about two dozen stripped nucleated dwarfs in the range $-13 < M_B < -11$ mag in the central 200 kpc projected distance of the Virgo cluster. A comparable number may be expected for the Centaurus cluster given its similar mass. The completeness of our survey within 200 kpc (16′) projected radius is about 12%, induced by 29% slit allocation completeness and about 40% area coverage. Formally, we would thus expect 3 ± 2 stripped dwarf galaxies with $M_B < -11$ mag ($M_V < -11.5$ mag). This number is too small to support the hypothesis that the slight overpopulation seen in Fig. 5 for bright luminosities is caused by stripped dwarfs.

Finally, we compare the total number of 27 compact objects with that expected from the GCLF. Our faint magnitude cut of $M_V = -10.9$ mag restricts us to $0.5\,^{+0.35}_{-0.2}$% of all GCs, provided that their luminosity distribution is described by a Gaussian of width $\sigma = 1.3 \pm 0.1$ mag and turn-over magnitude $M_V = -7.4 \pm 0.2$ mag. Under the null hypothesis that our compact objects are all explained by the GC system, we would deduce a total number of GCs in the surveyed area of $\frac{27}{0.005 \times C} = \frac{5400}{C} = \frac{5400}{0.28} = 19\,300^{+12900}_{-8260}$, where $C = 0.28$ is the completeness of our survey in the magnitude range where compact objects are discovered. We can now estimate which specific GC frequency $S_N = N_{GC} \times 10^{0.4\times(15+M_V)}$ is required for the two main Centaurus galaxies NGC 4696 and NGC 4709 in order to produce a total amount of ∼20 000 GCs. We derive the total absolute magnitude of both galaxies from our *V*-band pre-images. Under the assumption of $(m - M) = 33.28$ mag, we obtain values of $M_V = -23.1$ mag for NGC 4696 and $M_V = -22.3$ mag for NGC 4709, in agreement with other literature estimates (e.g. Michard et al. 2005; Jerjen et al. 1997). In order to contain $19\,300^{+12900}_{-8260}$ GCs, both galaxies would require $S_N = 7.5^{+4.9}_{-2.3}$. This agrees with the S_N values of 7.3 ± 1.5 (NGC 4696) and 5.0 ± 1.3 (NGC 4709) derived in Mieske et al. (2005) for the central regions of both galaxies (radii below 2′).

We conclude that the luminosity distribution and number of compact objects are consistent with the GC systems of NGC 4696 and NGC 4709.

4.2. Spatial distribution

In this sub-section we compare the cumulative radial distribution of the compact objects with that of dEs and of GCs.

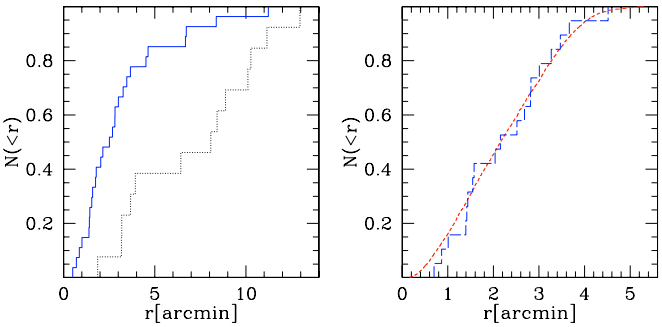

Fig. 6. Comparison of cumulative radial distributions of various object samples. *Left panel*: Centaurus compact objects are indicated by the (blue) solid histogram. The sample of 13 dwarf ellipticals is indicated by the (black) dotted histogram. For this plot, the radial distance was calculated with respect to NGC 4696 for the Cen30 members and with respect to NGC 4709 for the Cen45 members. The samples of compact objects and dEs have identical parent distributions at the 0.2% confidence level according to a KS-test. *Right panel*: the short dashed red line is the distribution of GC candidates around NGC 4696 from Mieske et al. (2005), see Fig. 1. The long dashed blue histogram is the distribution of compact objects restricted to the same field as the GC candidate sample. According to a KS test, both samples stem at 98% probability from the same parent distribution.

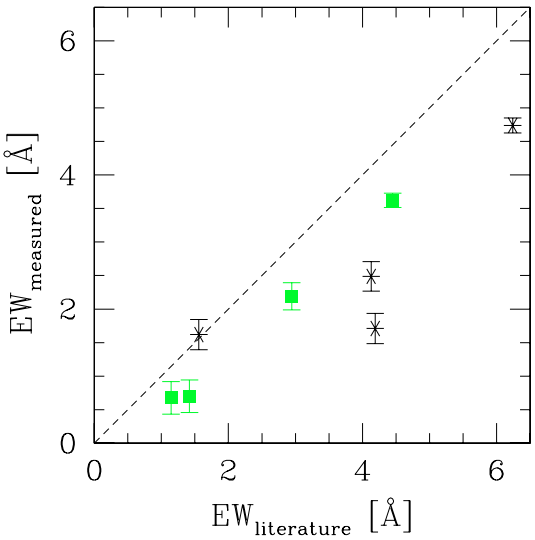

Fig. 7. Comparison between measured and literature Lick index values for the four Lick standard stars included in our observations. Index ⟨Fe⟩ is indicated by green solid squares, Mgb by black asterisks. Literature data is from Worthey et al. (1994). The dashed line indicates the identity.

Figure 6 shows that the compact objects are clearly more concentrated towards the central cluster galaxies than are the dEs included in our study. Selection effects regarding the dE sample should not significantly influence this finding, given that the dEs were selected from a homogeneous source catalog (Jerjen et al. 1997). Note that the stronger clustering of the compact objects does not exclude that they originate from dEs, since tidal stripping is expected to preferably affect dEs with smaller apocentric distances (Bekki et al. 2003).

For comparison with the genuine GC population, we use the deep FORS *VI* photometry from Mieske et al. (2005). The central FORS pointing of our previous study practically matches the area covered by the VIMOS quadrant centred on NGC 4696 (see Fig. 1). Since most of the candidates were detected in that quadrant, a direct comparison is possible. To define the GC candidate sample in the FORS observations, we restricted the colour range to $0.7 < (V - I) < 1.4$ mag (see Sect. 2.1) and the magnitude range to $-7.9 > M_V > -10.9$ mag. The bright magnitude cut makes the GC candidate sample disjunct from the compact object sample, the faint magnitude cut is due to the completeness limit. Figure 6 shows that the radial distribution of compact objects agrees very well with that of the GC candidates. The KS test gives a probability of 98% that both samples have identical parent distributions.

We thus conclude that the radial distribution of compact objects is consistent with that of the globular cluster system.

4.3. Abundances

Line index measurements of the 27 confirmed Centaurus compact objects, the 13 dEs, and the four Lick standard stars were performed with standard IRAF routines within the ONEDSPEC package. We derived Lick indices using the pass-band definitions of Trager et al. (1998). The instrumental resolution of 10–12 Å is slightly worse than the Lick resolution of 8–9 Å. The pass-bands were red-shifted according to the radial velocity of each investigated object.

For the four Lick standard stars, we compare in Fig. 7 our equivalent width (EW) measurements of both Mgb and ⟨Fe⟩ with the literature values (Worthey et al. 1994). We determine a global offset of -0.69 ± 0.08 Å for ⟨Fe⟩ and -1.39 ± 0.53 Å for Mgb. The correction is quite uncertain for Mgb, mainly due to one outlier (HD148816). We have gone back to the raw spectrum, but did not find artefacts that would have inhibited a correct index measurement for this source. Furthermore, the S/N was sufficiently high (≥50) for all four Lick standards. We re-measured the line indices for continuum normalised spectra, for logarithmic re-binnings, and for spectra extracted with a task outside the VIMOS pipeline (apall in the IRAF package twodspec). However, all this did not change the index values by more than ∼0.2 Å, and did not remove the outlier. We therefore apply the offsets resulting from the mean of all four Lick standards to the measured indices of compact objects and dEs.

In Fig. 8 we plot the correspondingly corrected ⟨Fe⟩ and Mgb line index EWs against each other. In the plot we also indicate the global uncertainty of the Lick calibration for ⟨Fe⟩ and Mgb. We sub-divide the Centaurus compact object sample into a high and low S/N sub-sample using $S/N = 30$ as limit. This roughly corresponds to a magnitude limit of $M_V = -11.6$ mag, see Fig. 9. We furthermore show literature line index measurements for Fornax and Virgo UCDs (Mieske et al. 2006a; Evstigneeva et al. 2007), Centaurus dEs (this paper), and Fornax and Virgo dEs (Geha et al. 2003). We overlay three model grids from Thomas et al. (2003), corresponding to a 12 Gyr single stellar populations with $[\alpha/\mathrm{Fe}] = 0$, 0.3, and 0.5 dex. The UCDs in Fornax, the Centaurus compact objects with high S/N, and the dEs in all three environments show roughly solar α abundances. The UCDs investigated in Virgo show in contrast super-solar abundances, between 0.3 and 0.5 dex. Assuming the IMFs are roughly similar, this implies that Virgo UCDs have had a more truncated star formation history than the other samples, in line with the galactic bulge population of globular clusters (e.g. Puzia et al. 2002; Barbuy et al. 1999; McWilliam & Rich 1994; Carretta et al. 2001 2007; Gratton et al. 2006).

It is interesting to note that also the low S/N Centaurus compact objects appear to show super-solar α values, albeit at a

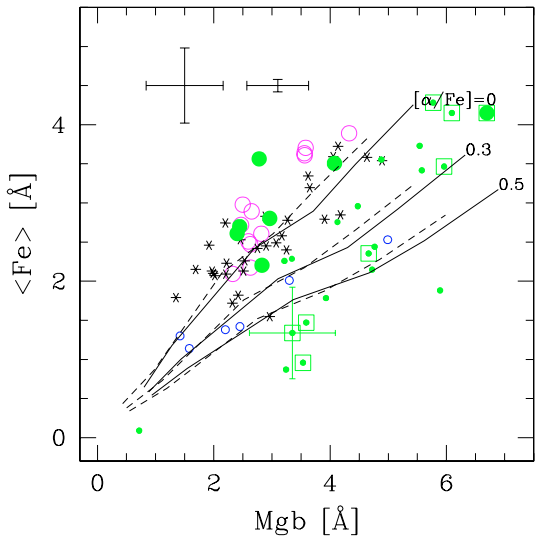

Fig. 8. Lick index ⟨Fe⟩ plotted vs. Mgb. Large, green filled circles are Centaurus compact objects with $S/N > 30$, small green filled circles those with $S/N < 30$. At the top, the left error bar indicates the average statistical uncertainty of our (green) data points, while the right error bar indicates the global uncertainty of our Lick calibration (see text). Sources surrounded by a solid square indicate those with HST imaging available (see Sect. 4.5). The source with an attached error bar is the most extended of those compact objects (see Sect. 4.5). Asterisks indicate values for central regions of dwarf elliptical galaxies, comprising the 13 Centaurus cluster dEs included in our study, and Fornax and Virgo dEs from Geha et al. (2003). Blue open circles are Virgo UCDs from Evstigneeva et al. (2007). Magenta open circles are the Fornax UCDs (Mieske et al. 2006a). The solid (dashed) lines indicate SSP models by Thomas et al. (2003) for an assumed age of 12 Gyr (4 Gyr) and the three indicated [α/Fe] values. Metallicities are from bottom to top −2.25 to 0.67 dex.

considerable scatter. We have tested whether the corresponding low ⟨Fe⟩ values may be artifacts of the lower S/N. For that we combined rest-frame corrected spectra to a higher S/N master spectrum, and compared the line index of the combined spectrum to the mean of the single indices. We did this for 4 sets of 3 spectra in different S/N ranges from $S/N \sim 18$ to $S/N \sim 45$. We found only very small differences of order 0.05 Å between the combined index and the averaged index, indicating that lower S/N may not be the reason for the apparent difference in α values to the brighter Centaurus compact object. However, deeper data with $S/N \geq 30$ (requiring on-source integration of about 1 night) are certainly required to confirm the possible trend of α abundance with luminosity.

In Fig. 9 we plot the logarithm of the [MgFe] index ([MgFe] = $\sqrt{\text{Mgb} \times \langle\text{Fe}\rangle}$) against luminosity for compact objects in Centaurus, Fornax and Virgo. The [MgFe] index is a good metallicity indicator (e.g. Puzia et al. 2002), given that it is practically insensitive to changes in α element contents (e.g. Thomas et al. 2003). We also indicate an estimate of the corresponding [Fe/H]. For this we use for [Fe/H] < −0.4 dex the empirical calibration between [Fe/H] and [MgFe] derived by Puzia et al. (2002) from galactic GCs. For [Fe/H] > −0.4 dex we adopt an extrapolation of the form $[\text{Fe/H}]_* = a + b \times \log(\text{MgFe})$ that matches the calibration for [Fe/H] < −0.4 dex. This is of course only a rough estimate whose systematic uncertainty is of the order 0.2–0.3 dex. The resulting mean $[\text{Fe/H}]_*$ of the Centaurus compact objects is −0.14 ± 0.06 dex (−0.08 ± 0.07 dex for the dominating Cen30 component, −0.39 ± 0.10 dex for Cen45). This is consistent with the typical metallicity of the metal-rich globular cluster sub-population (see e.g. Cohen et al. 2003; Peng et al. 2006). On a relative scale, the mean metallicity of the Fornax UCDs is indistinguishable from the Centaurus compact objects, but slightly higher than the metallicity range of the Virgo UCDs.

4.4. Kinematics

There is no spectroscopic data set of the Globular Cluster System in Centaurus available. Also, measurements of the field star velocity dispersion in NGC 4696 or NGC 4709 (Michard et al. 2005; Blakeslee et al. 2001) do not extend to large radii. The compact objects' kinematics can therefore only be compared directly with that of the cluster galaxy population. We subdivide the sample of compact objects into Cen30 and Cen45 at a limiting radial velocity of 4000 km s^{-1} (see Fig. 10).

Figure 10 shows that the mean velocity of the Cen30 and Cen45 components agree with the velocities of the respective central galaxies. The velocity dispersion of the 21 Cen30 compact objects is $433\ ^{+153}_{-98}$ km s^{-1}, where error ranges refer to a 95% confidence interval (2σ). This value is lower at the 4σ level than the dispersion of 738 km s^{-1} of the Cen30 early-type galaxies from Stein et al. (1997). The velocity dispersion of the six Cen45 compact objects is $288\ ^{+315}_{-95}$ km s^{-1}, indistinguishable to within its large error range from the dispersion of 345 km s^{-1} of the Cen45 early-type galaxies.

The lower velocity dispersion of the Cen30 compact objects as compared to the cluster galaxy population is consistent with the more centrally clustered distribution of the former. It indicates that the compact objects are associated more to the central galaxies than to the overall cluster potential.

4.5. Structural parameters

Out of the 27 compact objects detected in the CCOS, eight have archival HST imaging available. Six objects are found in one ACS pointing of NGC 4696 (Proposal 9427, PI Harris), while the two remaining sources are contained in two WF chips of one WFPC2 pointing (Proposal 6579, PI Tonry). Two example thumbnails are shown in Fig. 11. We use these images to estimate their sizes. To this end we use the program KINGPHOT (Jordán et al. 2004, 2005), which was already successfully applied to measure half-light radii r_h of GCs in Virgo and Fornax (Jordán et al. 2005, 2007). At the distance of the Centaurus cluster (assumed to be 43 Mpc), the resolution limit of the ACS images in terms of half light radius corresponds to ∼2.5 pc, i.e. about the typical value of GC r_h. The limit of the WF images is ∼5 pc. The resulting r_h estimates are listed in Table 1. Figure 12 plots M_V vs. r_h in pc measured on the HST images for the eight Centaurus compact objects. Over-plotted are HST based size estimates for compact objects in other environments: Fornax, Virgo, and the Local Group. The largest Centaurus compact object (CCOS J1248.74-4118.58) has a half-light radius of about 30 pc. Seven further objects have much smaller sizes in the range 4 to 10 pc, which is only marginally larger than typical GC sizes.

5. Discussion

5.1. Can we identify a bona fide UCD sub-sample?

In several respects (luminosity distribution, total number, spatial distribution, kinematics) the compact object sample does not show significant differences compared to what is expected from

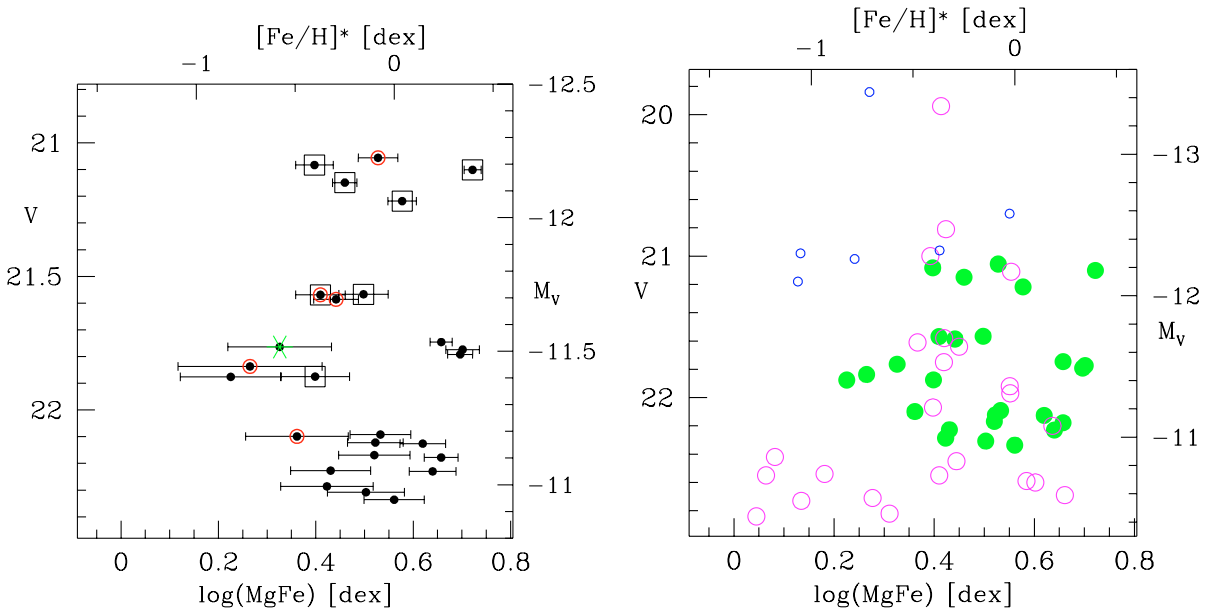

Fig. 9. *Left panel*: logarithm of the MgFe line index plotted vs. V for the Centaurus compact objects. The upper x-axis indicates an estimate of the corresponding [Fe/H], accurate to 0.2–0.3 dex, see text. Symbols surrounded by (red) circles indicate Cen45 members. The solid squares indicate spectra with S/N larger than 30. The green asterisk indicates the most extended object among the 8 sources with HST imaging (see text). *Right panel*: Log (MgFe) plotted vs. V for three samples of compact objects. Green filled circles indicate the Centaurus compact objects from the left panel. Blue open circles are the Virgo UCDs (Evstigneeva et al. 2007). Magenta open circles indicate Fornax compact objects (Mieske et al. 2006a).

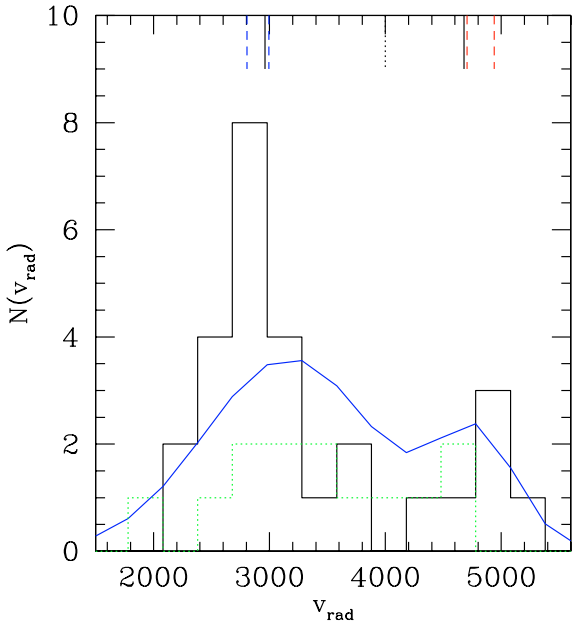

Fig. 10. Radial velocity histogram of Centaurus compact objects (solid line). The (blue) curve indicates the expected velocity distribution if the Cen30 and Cen45 sample had mean velocities and velocity dispersion identical to the early-type galaxy population in both sub-clusters (Stein et al. 1997). The dotted tick at 4000 km s^{-1} indicates the adopted separation between Cen30 and Cen45. The two solid ticks indicate the radial velocities of NGC 4696 (2960 km s^{-1}, NED) and NGC 4709 (4680 km s^{-1}, NED). The dashed ticks indicate the $\pm 1\sigma$ range of the measured radial velocities for compact objects in Cen30 and Cen45, respectively. The dotted (green) histogram shows the velocity distribution of the 13 dwarf elliptical galaxies included in our sample.

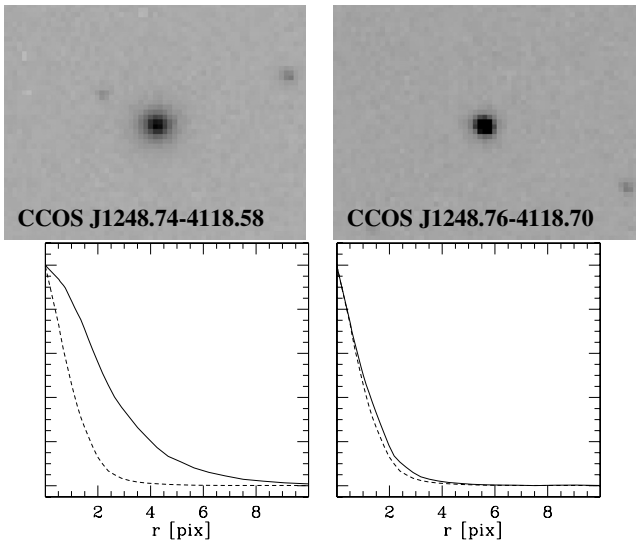

Fig. 11. *Top*: Two 3″ × 2.5″ HST archival image excerpts of Centaurus compact objects (a total of 9 objects have HST imaging available, see text). The images are from an ACS image in the *F*435*W* filter (Proposal 9427, PI Harris) with matched intensity cuts. Object CCOS J1248.74-4118.58 is the largest source of the sample, object CCOS J1248.76-4118.70 the smallest one (see also Fig. 12). *Bottom*: arbitrarily normalised radial intensity profile of both sources, compared to a stellar PSF (dashed line).

the globular cluster population. That is, based on those properties we are not able to identify a separate sub-population of UCDs.

What can we say about our compact object sample regarding sizes and abundances?

5.1.1. Sizes

Only one of the nine compact objects with HST imaging has a large size of r_h = 30 pc that clearly separates it from the typical

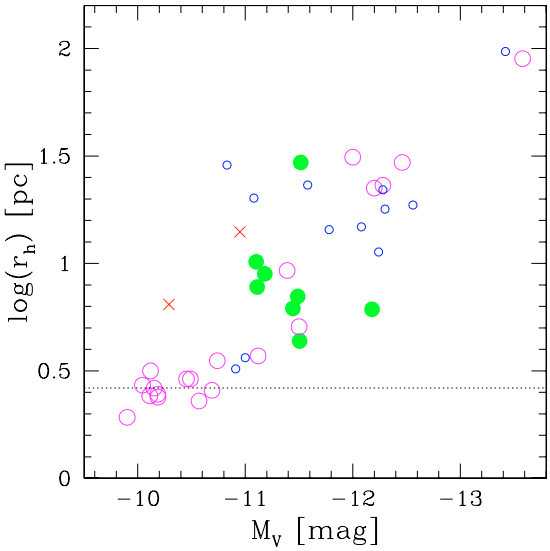

Fig. 12. HST based half light radius measurements of compact objects in various environments plotted vs. their absolute magnitude M_V. Green filled circles indicate Centaurus compact objects (this paper). The dotted line indicates the resolution limit of the Centaurus ACS images. This value ($r_h \simeq 2.5$ pc) also corresponds closely to the average GC size. Magenta open circles indicate Fornax compact objects from Mieske et al. (2006a) and Evstigneeva et al. (2007). Blue open circles are Virgo UCDs from Evstigneeva et al. (2007) and Haşegan et al. (2005). Red crosses are the Local Group compact objects ωCen (fainter) and G1 (brighter).

range of GC sizes. This object CCOS J1248.74-4118.58 truly classifies as an ultra-compact dwarf galaxy. In logarithmic space, its size is right between those of GCs and dwarf spheroidal galaxies (Mateo et al. 1998).

The overall size distribution of the Centaurus compact objects fits into the picture outlined in Haşegan et al. (2005) and Mieske et al. (2006a): for $M_V < -11$ mag the sizes of compact objects start to deviate from the typical GC values towards larger sizes. This may indicate that those large sources are the merger of several single star clusters (Kissler-Patig et al. 2006; Bekki et al. 2004; Fellhauer & Kroupa 2002). The magnitude range of the Centaurus compact objects is too small and their size scatter too large to confirm a *trend* of increasing size with luminosity, as it is found for Fornax and Virgo. This is partially due to the fact that we do not detect a very bright and large UCD with $M_V \simeq -13.5$ mag as in Fornax and Virgo. However, our survey completeness of 30% still allows at 95% confidence for 3–4 sources in the bright magnitude regime where no compact objects are found. We have to substantially increase our survey completeness to make firm statements on the size (and mass) range of UCDs in Centaurus.

5.1.2. Abundances

Our Centaurus sample does not show any obvious break in the metallicity distribution (Fig. 9) that would allow a sub-division in two groups of objects. The sample has a metallicity distribution whose mean agrees very well with the value of Fornax UCDs and that of the metal-rich GC subpopulation, with the scatter being somewhat larger than in Fornax. We note that our survey has an absolute magnitude limit of $M_V = -10.9$ mag, such that we would not be able to trace a metallicity break at $M_V = -11$ mag like that found for Fornax compact objects (Mieske et al. 2006a).

There may be a dichotomy in α abundance between bright and faint Centaurus compact objects, but this certainly needs confirmation with higher S/N data. Even if confirmed, this would not necessarily imply different formation mechanisms for bright and faint sources. The recently found colour-luminosity relation among bright blue GCs in various nearby GC systems (e.g. Harris et al. 2006; Strader et al. 2006; Mieske et al. 2006b) indicate that one may have abundance trends within one GC population. The findings of multiple or broadened main sequences in some massive Milky Way GCs (Bedin et al. 2004; D'Antona et al. 2005; Piotto et al. 2007) also point to the possibility of having complex star formation histories within massive GCs.

We note that another potential separation criterion between GCs and UCDs are M/L ratios (Haşegan et al. 2005). However, our low-resolution spectra do not allow to measure intrinsic velocity dispersions. This would require several nights of on-source integration at significantly higher spectral resolution.

5.2. Clues to the formation of UCDs

The only bona fide UCD detected in our survey appears to have a super-solar [α/Fe] abundance, different to typical values found for the current population of dEs. When including the abundance analyses done for UCD populations in Fornax and Virgo, it thus appears that today's dwarf elliptical galaxy population is not the parent population of most UCDs. The stellar super cluster scenario (SSC) (e.g. Fellhauer & Kroupa 2002) is a conceivable possibility for the formation of UCDs, also because young and very massive super-clusters – the possible UCD progenitors – can be observed in various environments today (e.g. Kissler-Patig et al. 2006; Bastian et al. 2006; Cortese et al. 2007). One would not expect too metal-poor SSCs given that they are created by already pre-processed material. This fits to the metallicities estimated for most of the UCDs. The scenario seems especially plausible for the Centaurus cluster, which is believed to have had a quite busy merger history (e.g. Furusho et al. 2001).

6. Conclusions

In this paper we have presented a search for ultra-compact dwarf galaxies in the Centaurus galaxy cluster. We acquired spectroscopic redshifts of about 400 compact object candidates with $19.2 < V < 22.4$ mag ($-14.1 < M_V < -10.9$ mag at the distance of Centaurus) with VIMOS@VLT. We find 27 compact objects (21 in Cen30, 6 in Cen45) with radial velocities consistent with Centaurus, covering an absolute magnitude range $-12.2 < M_V < -10.9$ mag.

Most properties (e.g. number, luminosity distribution, spatial distribution) of the compact object sample can be explained by the globular cluster systems in Centaurus, such that it is difficult to identify a UCD sub-sample. Only one of the eight sources with HST imaging has a large size of $r_h \sim 30$ pc which clearly distinguishes it from normal globular clusters. We consider this source the only bona fide UCD detected in our survey. It has an α abundance well above that of typical dwarf elliptical galaxies, more in line with Galactic bulge globular clusters. For this source, creation as a merged stellar super cluster in a past galaxy merger event appears plausible. To further quantify the properties of Centaurus UCDs, a significant increase of our survey completeness is necessary.

References

Barbuy, B., Renzini, A., Ortolani, S., Bica, E., & Guarnieri, M. D. 1999, A&A, 341, 539
Bassino, L. P., Muzzio, J. C., & Rabolli, M. 1994, ApJ, 431, 634
Bastian, N., Saglia, R. P., Goudfrooij, P., et al. 2006, A&A, 448, 881
Bedin, L. R., Piotto, G., Anderson, J., et al. 2004, ApJ, 605, L125
Bekki, K., Couch, W. J., Drinkwater, M. J., & Shioya, Y. 2003, MNRAS, 344, 399
Bekki, K., Couch, W. J., Drinkwater, M. J., & Shioya, Y. 2004, ApJ, 610, L13
Bertin, E., & Arnouts, S. 1996, A&AS 117, 393
Blakeslee, J. P., Lucey, J. R., Barris, B. J., Hudson, M. J., & Tonry, J. L. 2001, MNRAS, 327, 1004
Bruzual, G., & Charlot, S. 2003, MNRAS, 344, 1000
Carretta, E., Cohen, J. G., Gratton, R. G., & Behr, B. B. 2001, AJ, 122, 1469
Carretta, E., Bragaglia, A., Gratton, R.G., et al. 2007, A&A 464, 967
Cohen, J. R., Blakeslee, J. P., & Côté, P. 2003, ApJ, 592, 866
Cortese, L., Marcillac, D., Richard, J., et al. 2007, MNRAS 376, 157
Côté, P., Piatek, S., Ferrarese, L., et al. 2006, ApJS, 165, 57
D'Antona, F., Bellazzini, M., Caloi, V., et al. 2005, ApJ, 631, 868
Drinkwater, M. J., Jones, J. B., Gregg, M. D., & Phillipps, S. 2000, PASA, 17, 227
Drinkwater, M. J., Gregg, M. D., Hilker, M., et al. 2003, Nature, 423, 519
Evstigneeva, E. A., Gregg, M. D., Drinkwater, M. J., & Hilker, M. 2007, AJ, 133, 1722
Fellhauer, M., & Kroupa, P. 2002, MNRAS, 330, 642
Furusho, T., Yamasaki, N. Y., Ohashi, T., et al. 2001, PASJ, 53, 421
Geha, M., Guhathakurta, P., & van der Marel, R. P. 2003, 2003, AJ, 126, 1794
Gratton, R. G., Lucatello, S., Bragaglia, A., et al. 2006, A&A, 455, 271
Harris, W., Whitmore, B. C., Karakla, D., et al. 2006, ApJ, 636, 90
Haşegan, M., Jordán, A., Côté, P., et al. (VCS team) 2005, ApJ, 627, 203
Hilker, M., Infante, L., Vieira, G., Kissler-Patig, M., & Richtler, T. 1999, A&AS, 134, 75
Hilker, M., Baumgardt, H., Infante, L., et al. 2007, A&A, 463, 119
Jerjen, H., & Dressler, A. 1997, A&AS, 124, 1
Jones, J. B., Drinkwater, M. J., Jurek, R., et al. 2006, AJ, 131, 312
Jordán, A., Blakeslee, J. P., Peng, E. W., et al. 2004, ApJS, 154, 509
Jordán, A., Côté, P., Blakeslee, J. P., et al. 2005, ApJ, 634, 1002
Jordán, McLaughlin, D. E., Côté, P., A., et al. 2006, ApJ, 651, L25
Jordán, A., Blakeslee, J. P., Côté, P., et al. 2007, ApJS, 169, 213
Kissler-Patig, M., Jordán, A., & Bastian, N. 2006, A&A, 448, 1031
Kundu, A., & Whitmore, B. 2001, AJ, 121, 2950
Le Fevre, Saisse, M., Mancini, D., O., et al. 2003, SPIE, 4841, 1670
Lotz, J. M., Miller, B. W., & Ferguson, H. C. 2004, ApJ, 613, 262
Mateo, M. L. 1998, ARA&A, 36, 435
McWilliam, A., & Rich, R., Michael., 1994, ApJS, 91, 749
Michard, R. 2005, A&A, 429, 819
Mieske, S., Hilker, M., & Infante, L. 2002, A&A, 383, 832
Mieske, S., Hilker, M., & Infante, L. 2004a, A&A, 418, 445
Mieske, S., Infante, L., Benítez, N., et al. 2004b, AJ, 128, 1529
Mieske, S., Infante, L., Hilker, M., et al. 2005, A&A, 430, L25
Mieske, S., Hilker, M., Infante, L., & Jordán, A. 2006a, AJ, 131, 2442
Mieske, S., Jordán, A., Côté, P., et al. 2006b, ApJ, 653, 193
Mieske, S., West, M. J., & Mendes de Oliveira, C. 2006c, Proceedings of ESO Astrophysics Symposia: Groups of Galaxies in the Nearby Universe, ed. I. Saviane, V. Ivanov, J. Borissova, [arXiv:astro-ph/0603524]
Peng, E. W., Jordán, A., Côté, P., et al., 2006, ApJ, 639, 95
Phillipps, S., Drinkwater, M. J., Gregg, M. D., & Jones, J. B., 2001, ApJ, 560, 201
Piotto, G., et al. 2007, ApJL, in press, [arXiv:astro-ph/0703767]
Puzia, T. H., Saglia, R. P., Kissler-Patig, M., et al. 2002, A&A, 395, 45
Reiprich, T., & Böhringer, H. 2002, ApJ, 567, 716
Schlegel, D. J., Finkbeiner, D. P., & Davis, M. 1998, ApJ, 500, 525
Stein, P., Jerjen, H., & Federspiel, M. 1997, A&A, 327, 952
Strader, J., Brodie, J. P., Spitler, L., & Beasley, M. A. 2006, AJ, 132, 2333
Thomas, D., Maraston, C., & Bender, R. 2003, MNRAS, 339, 897
Trager, S. C., Worthey, G., Faber, S. M., Burstein, D., & Gonzalez, J. J. 1998, ApJS, 116, 1
Worthey, G., Faber, S. M., Gonzalez, J. J., & Burstein, D. 1994, ApJS, 94, 687
Zinn, R., & West, M. J. 1984, ApJS, 55, 45

Online Material

Table 1. Properties of the 27 Centaurus compact objects detected in our survey, ordered by magnitude. Errors are given in parentheses. "CCOS" in the object identifier stands for Centaurus Compact Object Survey. The last column gives the half-light radius in pc estimated from HST archival imaging.

ID	RA (J2000)	Dec (J2000)	V_0	$(V-R)_0$	$v_{\rm rad}$ [km s^{-1}]	⟨Fe⟩ [Å]	Mgb [Å]	r_h [pc]
CCOS J1250.02-4121.45	12:50:01.23	−41:21:26.83	21.06	0.40	4835 (60)	2.76 (0.36)	4.13 (0.55)	
CCOS J1248.54-4119.64	12:48:32.64	−41:19:38.20	21.08	0.47	3854 (69)	2.20 (0.27)	2.83 (0.36)	
CCOS J1248.79-4117.15	12:48:47.61	−41:17:09.12	21.10	0.50	2882 (54)	4.15 (0.25)	6.69 (0.36)	6.12 (0.45)
CCOS J1248.06-4111.40	12:48:03.76	−41:11:24.30	21.15	0.58	2768 (89)	2.80 (0.20)	2.96 (0.27)	
CCOS J1248.54-4121.90	12:48:32.48	−41:21:54.07	21.22	0.51	3279 (75)	3.51 (0.30)	4.07 (0.42)	
CCOS J1248.70-4121.11	12:48:41.75	−41:21:06.76	21.57	0.50	2521 (123)	3.56 (0.40)	2.78 (0.57)	
CCOS J1250.11-4114.59	12:50:06.57	−41:14:35.28	21.57	0.45	4430 (66)	2.70 (0.35)	2.44 (0.47)	
CCOS J1249.71-4120.63	12:49:42.63	−41:20:38.04	21.59	0.43	5184 (55)	2.29 (0.35)	3.34 (0.48)	
CCOS J1248.79-4116.00	12:48:47.69	−41:16:00.11	21.75	0.46	3140 (63)	3.73 (0.28)	5.54 (0.40)	
CCOS J1248.74-4118.58	12:48:44.70	−41:18:35.03	21.76	0.44	2189 (114)	1.34 (0.59)	3.35 (0.74)	29.49 (0.64)
CCOS J1248.76-4118.70	12:48:45.56	−41:18:42.21	21.77	0.55	2828 (45)	4.15 (0.47)	6.09 (0.68)	4.36 (0.30)
CCOS J1248.74-4119.74	12:48:44.33	−41:19:44.37	21.79	0.40	3138 (56)	4.28 (0.35)	5.77 (0.49)	7.02 (0.25)
CCOS J1250.03-4122.68	12:50:01.77	−41:22:40.60	21.84	0.54	4538 (66)	0.96 (0.61)	3.53 (0.85)	6.18 (0.83)
CCOS J1248.63-4115.71	12:48:37.77	−41:15:42.37	21.87	0.39	2524 (88)	2.61 (0.47)	2.40 (0.65)	
CCOS J1249.07-4120.77	12:49:03.99	−41:20:45.96	21.88	0.37	2453 (140)	0.87 (0.39)	3.24 (0.51)	
CCOS J1249.36-4121.57	12:49:21.64	−41:21:34.16	22.09	0.42	2790 (96)	2.44 (0.58)	4.76 (0.76)	
CCOS J1249.99-4124.45	12:49:59.21	−41:24:27.18	22.10	0.36	5000 (80)	1.47 (0.62)	3.59 (0.88)	8.94 (1.31)
CCOS J1248.97-4120.01	12:48:58.25	−41:20:00.52	22.12	0.52	2962 (98)	1.88 (0.45)	5.89 (0.62)	
CCOS J1248.65-4120.34	12:48:39.28	−41:20:20.58	22.13	0.55	3303 (69)	3.55 (0.53)	4.88 (0.76)	
CCOS J1248.74-4118.95	12:48:44.11	−41:18:56.87	22.17	0.53	3213 (53)	2.35 (0.65)	4.66 (0.90)	7.77 (1.32)
CCOS J1248.70-4118.23	12:48:41.99	−41:18:13.77	22.18	0.48	2822 (55)	3.47 (0.43)	5.96 (0.60)	10.17 (0.98)
CCOS J1250.07-4121.16	12:50:04.49	−41:21:09.37	22.18	0.43	4952 (80)	0.09 (0.92)	0.72 (1.25)	
CCOS J1248.72-4121.23	12:48:43.02	−41:21:13.54	22.23	0.58	2582 (99)	2.26 (0.60)	3.21 (0.86)	
CCOS J1249.41-4118.64	12:49:24.85	−41:18:38.15	22.23	0.58	2206 (79)	3.42 (0.60)	5.58 (0.76)	
CCOS J1248.91-4117.70	12:48:54.64	−41:17:42.05	22.29	0.43	2909 (120)	1.78 (0.67)	3.93 (0.88)	
CCOS J1248.99-4118.08	12:48:59.65	−41:18:04.51	22.31	0.53	2806 (75)	2.15 (0.66)	4.72 (0.91)	
CCOS J1248.62-4120.63	12:48:37.13	−41:20:37.79	22.34	0.52	3741 (85)	2.96 (0.61)	4.48 (0.87)	